Magnetic Resonance Imaging 55 (2019) 145–152

Contents lists available at ScienceDirect

Magnetic Resonance Imaging

journal homepage: www.elsevier.com/locate/mri

Iron quantification in Parkinson's disease using an age-based threshold on susceptibility maps: The advantage of local versus entire structure iron content measurements

Sean K. Sethi[a,b,*], Shawn J. Kisch[c], Kiarash Ghassaban[b], Ali Rajput[d], Alex Rajput[d], Paul S. Babyn[c], Saifeng Liu[a], Peter Szkup[c], E. Mark Haacke[a,b,e]

[a] Magnetic Resonance Imaging Institute for Biomedical Research, Bingham Farms, MI 48025, USA
[b] Magnetic Resonance Innovations, Inc., Bingham Farms, MI 48025, USA
[c] The Department of Medical Imaging, The University of Saskatchewan and Saskatoon Health Region, 103 Hospital Dr, Saskatoon, SK S7N 0W8, Canada
[d] The Division of Neurology in the Department of Medicine, The University of Saskatchewan and Saskatoon Health Region, 103 Hospital Dr, Saskatoon, SK S7N 0W8, Canada
[e] Department of Biomedical Engineering, Wayne State University, Detroit, MI 48202, USA

A B S T R A C T

Background: Elevated brain iron has been observed in Idiopathic Parkinson's disease (IPD) within the deep gray matter. Using quantitative susceptibility mapping (QSM) and a thresholded high-iron region, we quantified iron content in the midbrain of patients with Parkinson's disease as a function of age.

Methods: We used MRI to scan 24 IPD patients at 3-Tesla. Susceptibility-weighted images were collected with the following parameters, TE: 6 and 20 ms, TR: 30 ms, FA: 15°, and resolution: 0.5 × 0.5 × 2.0 mm^3. QSM images were reconstructed from the source phase images. Whole-region and thresholded high-iron (RII) region boundaries for the Substantia Nigra (SN) and Red Nucleus (RN) were traced. Iron content was measured via mean susceptibilities and volumes, which were compared between the groups, as well as between right and left side of the structures within groups.

Results: Twenty patients with mild to moderate IPD were used in this study. For the SN, mean RII and whole-region iron and volumes were higher in the IPD group compared to HC, as well as mean RII for the RN, while no differences were seen between the groups when considering whole-region mean susceptibility bilaterally for the RN.

Conclusion: Using a two-region of interest analysis on QSM, we showed that abnormal iron occurs in IPD patients in the SN and with greater volumes compared to HC. This method may have application as a biomarker for disease diagnosis and early intervention.

1. Introduction

Idiopathic Parkinson's disease (IPD) affects approximately 0.1% to 0.3% of the population [1] and is currently the second most common neurodegenerative disease in the western world [2]. Given that the median onset age of IPD is about 50 years, the percentage of the affected population is expected to rise in the coming decades due to an increase in aging population worldwide.

The most prominent pathological hallmark of IPD patients is the degeneration of dopamine-producing cells in the Substantia Nigra (SN) [3–6] as well as a reduction of dopamine levels in the corpus striatum [7]. Dopamine acts like a messenger between the two areas resulting in smooth, controlled movements. Neuronal losses in the locus coeruleus [8] and the appearance of Lewy bodies within other regions of the brain such as the brainstem [9] may contribute to other symptoms associated with IPD. Symptom severity for the disease is commonly monitored using the Unified Parkinson's Disease Rating Scale (UPDRS) score [10,11]. Both clinicians and researchers use the motor section in particular to track a patient's progression of a patient's symptoms or the benefits of a given therapy in an objective manner. Advances in medical imaging have led to a greater understanding of the pathogenesis of IPD and have stimulated the development of potential disease-modifying therapies [12,13]. Unfortunately, the cause of the degeneration of dopamine-producing cells in IPD patients is still unknown.

Given that IPD is generally a late-onset disease and iron levels in the brain are known to rise with age [14], there has been strong interest in determining a potential correlation between IPD and levels of iron in specific deep gray matter structures [15,16]. This concept dates back several decades to Dexter et al.'s work [17] showing that total iron levels are elevated in the basal ganglia of IPD patients. MRI has been employed to measure iron content of the brain using a number of methods, which have focused on the measurement of T2* relaxation

* Corresponding author at: 30200 Telegraph Road #140, Bingham Farms, MI 48025, USA.
E-mail address: sethisea@gmail.com (S.K. Sethi).

https://doi.org/10.1016/j.mri.2018.10.001
Received 11 April 2018; Received in revised form 29 August 2018; Accepted 6 October 2018

time and how it is affected by susceptibility [18]. In general, iron levels in IPD have been found to be elevated in the SN [19], putamen [20], caudate nucleus [17] and thalamus [21] while decreasing in the Globus Pallidus (GP) [17]. Conventionally, R2* relaxation rate mapping is used to measure iron content, however, its accuracy is dependent on selected imaging parameters, orientation, and signal-to-noise ratio (SNR) [22], [23]. Phase has also been used to measure iron content in neurodegenerative disease [24], however, it is sensitive to the geometry of the object. R2* also only uses magnitude data, whereas phase information is actually more sensitive to iron content. Susceptibility Weighted Imaging (SWI) is a widely-used GRE technique which not only uses MRI signal magnitude, but also signal phase to generate image contrast. It can be used to improve contrast in iron-rich brain regions such as the GP and SN [25–28].

Quantitative Susceptibility Mapping (QSM) is a fairly new post-processing technique with the ability to quantify iron over the entire brain and has specific advantages over R2* and phase because it is independent of MR imaging parameters such as TE, field strength, geometry, and position in the magnetic field [29,49]. Recently, QSM has been used on PD patients to show greater sensitivity in detecting iron in the SN [30–33] and other deep gray matter nuclei [31–33] compared to R2*, as well as showing stronger correlation with clinical scores [30–32]. Liu et al. has used QSM on a large cohort of healthy controls, and shown an increasing mean susceptibility within deep GM structures over time, as well as a robust susceptibility-age baseline in a thresholded high iron content region in these structures [34] raising the questions of whether there is a difference between iron levels in healthy controls and IPD patients. We hypothesize that using a thresholded method to quantify iron in the midbrain of IPD subjects will have a more robust correlation with age compared to using the whole region. We also hypothesize that abnormal iron levels will correlate with the severity of IPD based on the Hoehn and Yahr Stage and other clinical scores. Additionally, we investigate the difference between iron deposition in the midbrain of IPD patients and healthy controls from Liu et al.'s study [34]. The ability to accurately measure non-heme iron in the brain may facilitate a better understanding of disease progression and may help in treatment outcome.

2. Methods

2.1. Data collection

This research study was approved by the University of Saskatchewan's Research Ethics Board for clinical investigation. Informed consent was obtained in writing from all subjects prior to clinical trial registration. Twenty-four (24) patients with clinically diagnosed IPD were recruited upon the recommendation of a neurologist from the University of Saskatchewan. A neurologist initially evaluated all patients using a questionnaire and a clinical assessment (performed prior to the patient taking any medications). This included administration of a UPDRS – Motor Assessment, MME – Mini Mental Status Examination and ADL – Activities of Daily Living assessment on IPD patients at most 1 year prior to and one year after the MRI. All patients were chosen to have a Hoehn and Yahr stage score of 1, 1.5 or 2, as patients with higher scores have more severe disease and generally cannot tolerate holding still for the duration of the MRI scan.

Participants were excluded if they had medical implants that were not MRI-compatible, implanted vascular devices such as cardiac stents, a history of kidney disease, liver disease, were diabetic, had severe hypertension or other vascular disorders such as stroke or heart attack. All IPD participants were screened for MR system compatibility and scanned using a Siemens 3 T Skyra MRI system (Siemens Healthcare, Erlangen, Germany) using a 20-channel head/neck coil. The MRI protocol included conventional clinical imaging and SWI imaging (see Table 1). Demographics and clinical characteristics are given in Table 2.

The controls in the paper are from a previous work [34]. A total of 188 subjects were enrolled and scanned of which 174 subjects ranging from 20 to 69 years of age were included. The imaging took place at Dalian First Affiliated Hospital on a 1.5 T GE scanner (HD, General Electric, Milwaukee, WI) with signed informed consent approved by the Institutional Review Board. Collecting data took about 6 months. Exclusion criteria were: history of neurological or psychiatric conditions; head trauma; drug and alcohol abuse; and brain surgery. These participants did not show any focal parenchymal loss, infarction, resection, or large hyperintensities in their brain on T2-weighted images.

Table 1
Imaging parameters for this study.

	T2 TSE	T1 MPRAGE	3D FLAIR	3D SWI 2-Echo
Orientation	Transverse	Transverse	Sagittal	Transverse
TR (ms)	7080	1750	6000	30
TE (ms)	77	2.98	397	6/20
Flip angle	120°	9°	120°	15°
Resolution (mm × mm)	0.5 × 1.0	0.5 × 1.0	1.0 × 1.0	0.5 × 0.5
Slice thickness (mm)	2	1	1	2
Bandwidth (Hz/pixel)	222	180	781	407/121

2.2. Data processing and statistical analysis

2.2.1. Data processing

Data processing was performed using an in-house Matlab toolbox (SMART, The MRI Institute for Biomedical Research, Detroit, MI). Magnitude and phase images were reconstructed from the original 20-channel data using the Echo Center Correction (ECC) algorithm which corrects the echo center shift caused by coil sensitivity induced phase components [35]. All QSM data were generated from the data collected at TE = 20 ms in four steps: brain extraction [36], phase unwrapping [37], background field removal with a kernel size of 6, and a deconvolution size of 0.05 [38], and an iterative thresholded k-space division for generating the susceptibility maps [39]. Upon QSM generation: 1) 3D multi-slice regions of interest for the SN and RN were manually traced (both the magnitude and phase images were used to ensure that the boundaries for each region were properly drawn) and the mean susceptibility values (for the whole-region analysis) were then extracted for each structure and 2) as introduced in Liu et al.'s study, an automatic threshold-based technique based on age, was applied to the QSM maps in order to define the high-iron content voxels, also known as region-II (RII), lying higher than the upper 95% prediction intervals in the susceptibility-age whole-region analysis [34]. Mean susceptibility values in RII (i.e. regional analysis) were extracted for each nucleus [34]. QSM data from Liu et al. were used as a reference data to compare with IPD [34].

2.2.2. Statistical analysis

All statistical analyses were performed using SPSS 20.0 (IBM Corp., Armonk, New York). Two-tailed *t*-tests were run to compare both RII volume and whole-region volume between the two groups and bilaterally within each group. Regression statistics for the IPD and HC groups were calculated to obtain correlation coefficients, slopes, and intercepts of the age vs RII iron content, and age vs whole-region iron content. Further, we used the confidence intervals from the age vs. RII mean susceptibility plots from the HC to compare to the IPD group. To address the concern for the limited sample size, we have simulated means for an age-matched group of HC based on the ages of the IPD group. We used ages of the IPD cohort as an independent variable to calculate the mean susceptibility based on the age vs. RII mean susceptibility linear regression equations. Following this, we performed a paired *t*-test between the IPD means and the simulated means for the HC group. p-Values < 0.05 were considered significant.

Table 2
IPD subject descriptors.

	Females (males)	Age (years)	Duration of IPD (years)	Hoehn and Yahr stage	MME	ADL
$N = 24$	5 (19)	67.2 ± 10	7.1 ± 5	2.0 ± 0.3	28.5 ± 2	90.0 ± 10

2.2.3. Intra-rater reliability assessment for structure boundary demarcation

To test for inter-rater reliability for manual tracing of regions, the intra-class coefficient was computed under a random raters' assumption [40]. Mean whole-region susceptibility, RII susceptibility, and volumes were assessed for both right and left sides for each structure. Three raters met a reliability standard of > 0.85 for all mean susceptibility measurements, as well as volumes for each structure and side.

3. Results

3.1. Mean susceptibilities and volumes for midbrain RII and whole regions

3.1.1. Comparison of iron content between right and left sides for the IPD group

Data from 20 mild to moderate IPD patients aged 67.0 ± 10 years were used in this analysis. Four patients were excluded from the analysis due to poor data quality. For the IPD group, whole-region susceptibility means for the right and left SN were 137 ppb (SE = 8) and 142 ppb (SE = 7), respectively, and were not significantly different ($t(19) = -0.87$, $p = 0.40$). Differences were seen between the RII means for the right (210 ppb, SE = 5) and left SN (228 ppb, SE = 6) ($t(19) = -6.1$, $p < 0.001$). For the RN, whole-region susceptibility means were similar between the right side 91.8 ppb (SE = 9) and the left side 80 ppb (SE = 10) ($t(19) = 2.03$, $p = 0.06$). For the right and left RN, RII susceptibility means did not differ; 177 ppb (SE = 5) and 175 (SE = 4), respectively ($t(19) = 0.75$, $p = 0.47$). Table 3 shows whole-region and RII susceptibilities bilaterally for each structure for the IPD and HC groups, as well as their volumes. No differences were observed between right and left volumes for both RII and whole-region SN and RN (all *p*s > 0.05) Fig. 1 shows an example of whole-region and high-region iron in HC and IPD subjects.

3.1.2. Comparison of iron content between IPD and HC groups

The IPD groups showed larger RII susceptibility in the SN compared to the HC in both the right (210 ppb vs. 184 ppb, $p < 0.001$) and left side (228 ppb vs. 193 ppb, $p < 0.001$), as well as for whole-region susceptibility (right: 137 ppb vs 93 ppb, $p < 0.001$; left: 143 vs. 105 ppb, $p < 0.001$). RII iron volumes were higher in IPD compared to HC for both right and left hemisphere (right: 151 mm^3 vs. 81 mm^3, $p < 0.001$; left: 228 mm^3 vs. 193 mm^3, $p = 0.001$); however, whole region volumes were similar between the groups ($p = 0.43$ for right, and $p = 0.52$ for left). Fig. 2 shows RII volume vs. age for the SN further highlighting the differences between the two groups. RII means were higher in the IPD group for RN susceptibilities (177 ppb vs. 157 ppb, $p < 0.001$; left: 175 ppb vs. 159 ppb, $p = 0.004$), while whole-region means between the groups were similar ($p = 0.08$ for right, $p = 0.84$ for left). Whole-region RN volumes for IPD were higher compared to HC for both sides ($p = 0.02$ for right, and $p < 0.001$ for left). However, no differences were observed between RII volumes for the RN between the groups ($p = 0.55$, $p = 0.51$). Figs. 3 and 4 show the age vs. mean susceptibility plots for RII and whole region for SN and RN, respectively. The linear regression lines for the HC groups are shown along with the 95% confidence intervals (dashed lines). Using the age vs RII susceptibility equation, we calculated the simulated RII SN means for the age-matched HC to be 196 ppb (SE = 1) and 207 ppb (SE = 1). Both simulated means were lower compared to the IPD cohort ($p = 0.001$ for both right and left side). (Table 4) shows the RII and whole-region means and volumes for the original data.

3.2. Disease state scores vs. mean RII susceptibility

Coefficients of correlation were assessed between disease state scores and RII mean susceptibilities for each side for the SN. Results showed weak correlations between susceptibility and years since diagnosis (right: 0.22, $p = 0.35$; left: 0.15, $p = 0.54$), weak negative correlations between susceptibility and average MME (right: −0.38, $p = 0.11$, left: −0.26, $p = 0.29$), as well as between susceptibility and average ADL (right: −0.42, $p = 0.076$; left: −0.30, $p = 0.21$).

4. Discussion

The main finding in this study is that the means and volumes of abnormal high iron deposition are elevated in IPD compared with HC bilaterally for the SN, as well as for the SN for the whole-region. Generally, variability is reduced and the robustness of the age vs. susceptibility plots improved when using the RII method for both RN and SN. When using the upper 95% confidence intervals for the RII mean susceptibility vs. age plots for HC as a cutoff, three IPD cases lay above the upper interval for the right SN side and 7 cases lay above for the left SN. Using a simulated RII means based from the HC RII regression lines, we observed that the IPD also show elevated mean susceptibilities compared with the mean values expected from the age matched HC

Table 3
Mean RII (high-iron region) and whole-region susceptibility (χ) (in ppb) and volume (in mm^3) ± standard deviation by structure for Idiopathic Parkinson's Disease (IPD) and healthy control (HC) subjects; χ = susceptibility.

		n	Right mean χ (ppb)	Right volume (mm^3)	*n*	Left mean χ (ppb)	Left volume (mm^3)
Substantia Nigra							
RII	IPD	20	210 ± 23	151 ± 81	20	228 ± 28	128 ± 65
RII	HC	155	184 ± 17	81 ± 60	162	193 ± 17	75 ± 64
Whole-region	IPD	20	137 ± 37	443 ± 53	20	143 ± 39	436 ± 59
Whole-region	HC	165	93 ± 26	429 ± 77	165	105 ± 28	425 ± 72
Red Nucleus							
RII	IPD	20	177 ± 21	56 ± 40	20	175 ± 19	37 ± 32
RII	HC	136	157 ± 23	40 ± 35	140	159 ± 23	42 ± 37
Whole-region	IPD	20	92 ± 40	239 ± 49	20	80 ± 44	240 ± 56
Whole-region	HC	169	78 ± 31	218 ± 37	169	82 ± 33	213 ± 38

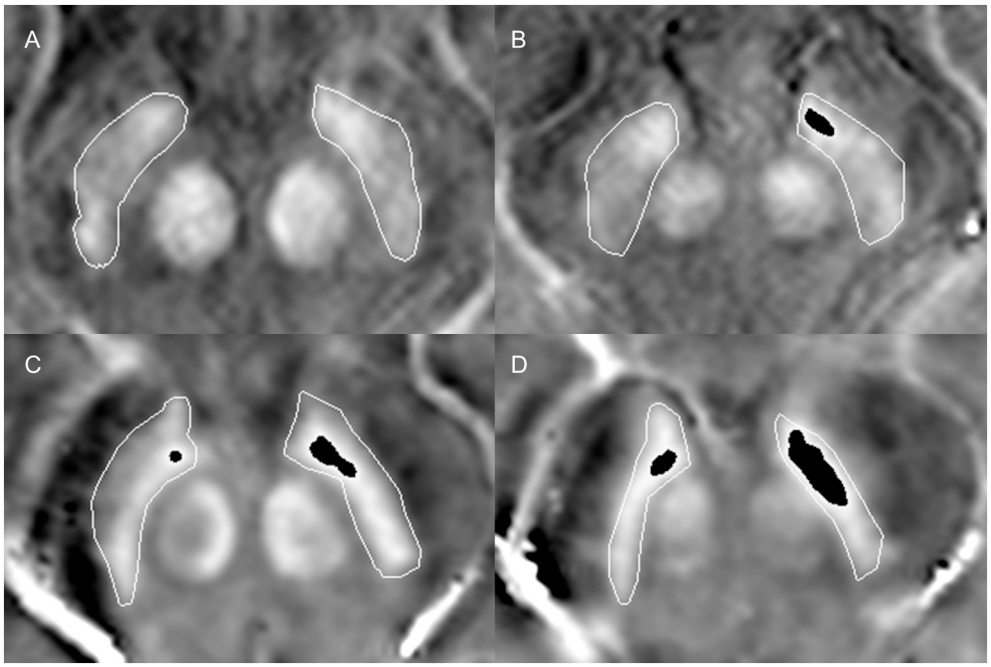

Fig. 1. Example quantitative susceptibility map result for an Idiopathic Parkinson's Disease (IPD) and a healthy control (HC) subject showing the Region-II (RII) iron for the Substantia Nigra (SN).
A–B: QSM of a 66 year old HC subject. Resolution: 0.47 × 0.47 × 3 mm^3. Slices go from the superior (A) direction to the inferior (B) direction. C–D: QSM of a 66 year old HC subject. Resolution: 0.5 × 0.5 × 2 mm^3. Slices go from the superior (C) to the inferior direction (D). Images show object tracings for the SN. Black regions within the boundaries denote abnormal iron which was thresholded above 2*SD of the regression line for age vs. mean susceptibility for the HC group.

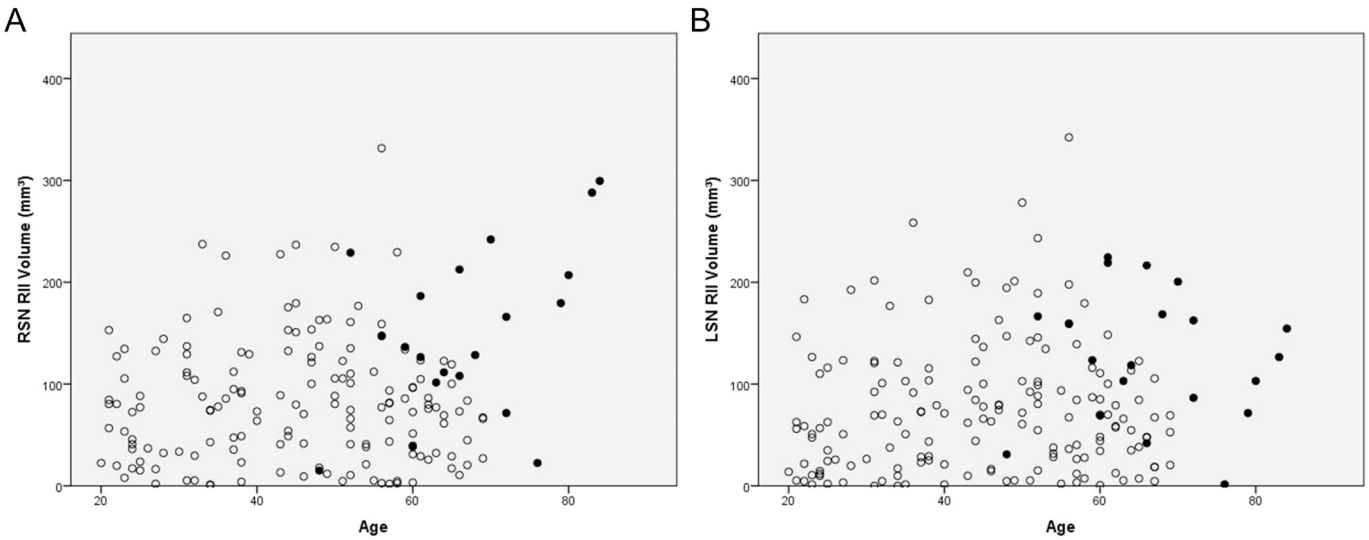

Fig. 2. A and B: Region-II (RII) volume (mm^3) vs. age plots for the right (A) and left (B) Substantia Nigra (SN). Solid circles: Idiopathic Parkinson's Disease (IPD), open circles: healthy controls (HC).

data. When considering the RN, only RII iron was higher for IPD patients. While some have reported increased iron deposition in the RN in postmortem patients, it may be due to the stage in the disease course. It has been suggested that the increase in iron may be due to the proximity of the RN to a high-iron SN, and not the RN itself [41]. Plots showing disease severity scores vs. RII susceptibility showed weak correlations (r^2 ranged from 0.02–0.18). Due to the small sample size, as well as the lack of variability in disease state, these results should be interpreted with caution until a larger and longitudinal, age-matched study is performed.

Elevated iron is a proxy marker for oxidative stress, which promotes the death of dopaminergic neurons in the SN for Parkinson's Disease. It is still disputed whether high iron is a cause of the disease or accelerates the disease course or is just a biomarker of tissue changes [42]. Both RII mean susceptibility vs. age regression lines for the SN suggest that the rates of abnormal iron deposition between HC and IPD may diverge as early as age 43, based on the intersection of the PD and HC lines for the right and left side. While the location of the RII iron was not part of this study, it is suggested that the locations may be predominantly in the *pars compacta* for early disease subjects, and the *pars reticulata* in later stage subjects [31]. Generally, the pattern of the high abnormal iron in our small cohort showed concentrations close to the draining vein in the anterior part of the SN in the cranial slices, with the middle slices being very iron-rich. It has been suggested that iron may deposit antegrade to the draining vein in the basal ganglia and midbrain [34], however, more cases would be needed to verify this observation.

Several other QSM studies investigating the effects of susceptibility changes in the midbrain have claimed that iron deposition in the SN of PD patients is significantly higher than that of healthy controls. Guan and colleagues evaluated the SN on 40 controls vs. 60 PD patients, divided into early and late stage PD using QSM, and found regional differences in the SN dependent on the disease stage. Their group used a multi-echo approach to generate QSM, as well as the iterative inverse filter (iLSQR algorithm) which achieved a higher SNR and reduced

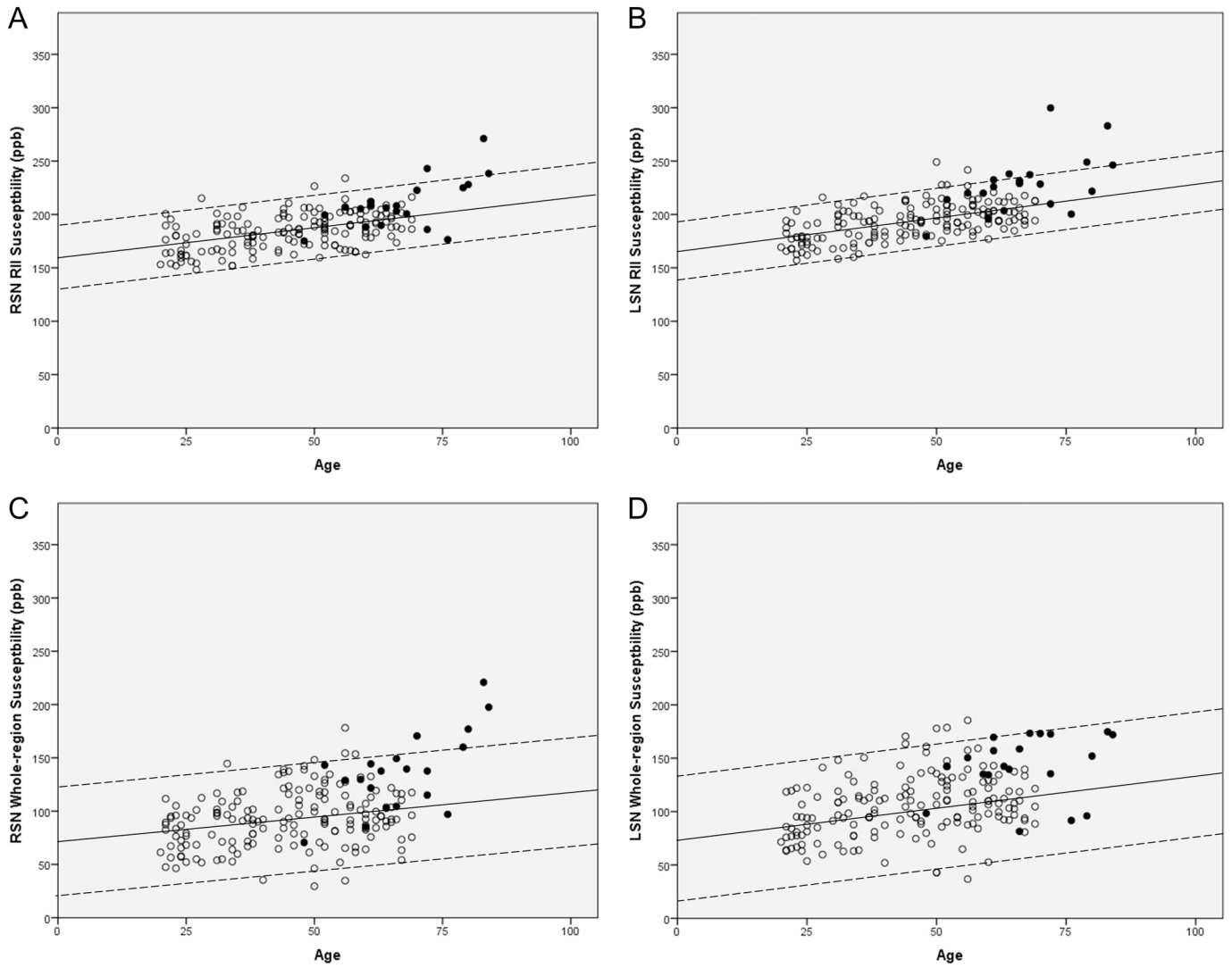

Fig. 3. A–D: Plots showing Region-II (RII) and Whole-region iron content as a function of age for the Substantia Nigra (SN).
A–B: Plots for RII susceptibility vs. age for the right SN (A) and left SN (B); C–D: Plots for whole-region susceptibility vs. age for the right SN (C) and left SN (D). Open circles: HC, solid circles: IPD.

streaking artifacts [31]. Our study used a single echo approach and was limited to studying only mild and moderate IPD subjects. A few additional studies have demonstrated increased iron content in the SN by comparing PD patients to matched healthy groups [30,32,33,43–47]. Lotfipour et al. used QSM maps generated from 7 T field strength to demonstrate that there is significantly higher iron content in the SN *pars compacta* (SNpc) [43]. Using other QSM techniques at different field strengths, other groups have also claimed elevated levels of iron deposition in the SNpc [30, 44–46]. In this study, we have come to similar conclusions particularly using the regional analysis which showed striking differences between PD patients and HC, although we did not separate the SNpc. The fact that rate of iron increases in PD is significantly greater than the HC population suggests that this RII high iron content approach may offer a more sensitive means to monitor disease onset. However, clearly not all IPD patients show high iron in the SN.

QSM is gaining momentum as the standard for measuring brain iron due to its high sensitivity and specificity. In our study, we used almost the same data processing algorithm as that used in Liu et al. [34]. The only difference between these two studies is that, in our work we used a spatial Laplacian unwrapping as opposed to the 3D phase unwrapping algorithm used in Liu et al. The performance of these different techniques was tested by Haacke and colleagues [29] on a 3D brain model and in vivo data and they concluded that the Laplacian unwrapping leads to almost the same result as the ideal unwrapped phase images without phase aliasing. One drawback of Laplacian unwrapping is that it may lead to unreliable phase near the edges of veins, in the context of this work, the vein nearest to the midbrain would be the basal vein of Rosenthal, although that did not affect our susceptibility measurements of the deep gray matter structures.

The accuracy of iron quantification may be affected by both the background field removal and the inverse problem solving steps in QSM data reconstruction. For background field removal, we used the SHARP algorithm, which has better accuracy in the central part of the brain than the edges of the brain. Hence, for the purpose of our study, this leads to more reliable estimates of the iron content in deep gray matter structures than using high-pass filtering. However, SHARP may still lead to a bias in the final susceptibility quantification [29]. Additionally, the thresholded k-space division (TKD) algorithm for solving the ill-posed inverse problem is known to cause under-estimation of the susceptibility. More advanced algorithms which utilize the geometry information extracted from magnitude, phase and susceptibility maps may help to further reduce this systematic under-estimation. In our study, we used the same k-space threshold as the one used by Liu et al.

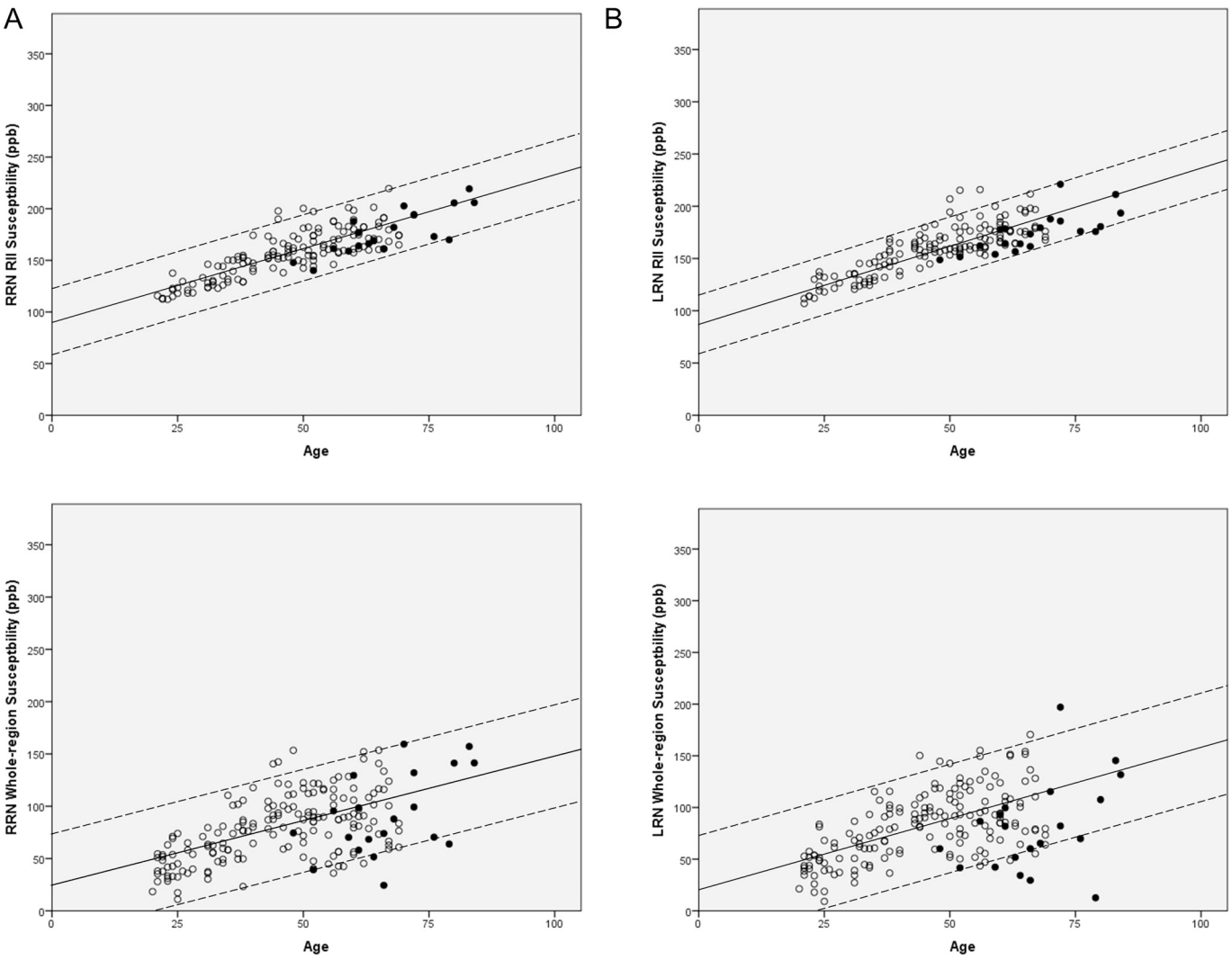

Fig. 4. A–D: Plots showing Region-II (RII) and Whole-region iron content as a function of age for the Red Nucleus (RN)
A–B: Plots for RII susceptibility vs. age for the right RN (A) and left RN (B); C–D: Plots for whole-region susceptibility vs. age for the right RN (C) and left RN (D). Open circles: healthy controls (HC), solid circles: Idiopathic Parkinson's Disease: (IPD).

Table 4
Linear regression coefficients for age vs. mean susceptibility, and regression line slopes for age vs. mean susceptibility (χ) for Region-II and whole-region Substantia Nigra (SN) and Red Nucleus (RN). Susceptibility values are in parts per billion (ppb). IPD: Idiopathic Parkinson's Disease, HC: healthy control, χ = susceptibility.

	IPD	HC	$\chi = \chi$/year * age			
			IPD		HC	
	R	R	χ/year	SE	χ/year	SE
RII RSN mean	0.62	0.47	1.45	0.4	0.56	0.1
Whole-region RSN mean	0.66	0.26	2.42	0.6	0.48	0.1
RII LSN mean	0.56	0.54	1.54	0.5	0.63	0.1
Whole-region LSN mean	0.18	0.30	0.54	0.7	0.60	0.1
RII RRN mean	0.79	0.81	1.67	0.3	1.44	0.1
Whole-region RRN mean	0.51	0.57	2.02	0.8	1.24	0.1
RII LRN mean	0.73	0.83	1.36	0.3	1.47	0.1
Whole-region LRN mean	0.40	0.60	1.75	1.0	1.38	0.1

and the systematic errors due to this TKD algorithms are expected to be the same in our study and the study by Liu and colleagues [34]. This enables an easy and consistent comparison between the results obtained in this study and in that earlier study.

There are several limitations in this study. First, we used a manual-tracing approach to draw the structures. This lends itself to subjectivity and can be time-consuming. While the raters met a reliability standard, variations in boundary tracing are mitigated by using an RII method, in that pixels of surrounding tissue or internal capsule with lower susceptibility will not be included making the iron measurement more robust. Secondly, the make, model, and field strength of the scanners involved differ between this work and Liu et al.'s work. The advantage of using QSM is that it is technically independent of field strength and TE. The QSM results from this 1.5 T data set has already been shown by Liu et al. to match the 3 T data from another study of 191 subjects scanned at 3 T by Li et al. [48]. QSM is a technique that depends on the phase from a gradient echo scan. The phase depends on the product of the field strength and echo time by collecting the data with an echo time of 40 ms at 1.5 T one obtains the same phase as collecting the data with an echo time of 20 ms at 3 T. After appropriate high pass or other filtering, the core phase information remains identical and hence one expects the susceptibility results to be identical. The sequences are generally the same to collect the data, and the processing algorithms are also similar to generate the maps. Third, differences in slice thickness between the two groups may also be a confounding factor, as thicker slices may lead to reduced susceptibility due to partial volume effects [34]. Fourth, the resolution for our images did not allow us to

demarcate the SNpc to detect iron increases as a proxy for neuronal loss. It would be of value to either take more time to obtain better resolution at 3 T or to collect data with a higher-field strength to have better SNR. Fifth, the limited sample size of the IPD is small and also yields low statistical power compared to the large number of controls, therefore the results should be interpreted with caution. In the future, we plan to recruit a larger cohort of subjects along with age-matched controls for a more proper analysis. Sixth, the IPD sample was mostly male and was limited to mild and moderate subjects, which in turn limited our ability to compare differences by gender, as well assess iron properties in severe subjects. Seventh, cusp artifacts due to scanner software rendered some of our IPD data unusable. While we were able to mitigate these effects on some cases by reconstructing the channel data with in-house software, it limited some of the structures we were able to measure, and hindered our ability to do multi-echo processing which may have increased SNR on QSM. The next generation software from this vendor has eliminated this problem.

5. Conclusion

Using a two-region of interest analysis on the QSM data, specifically focusing on high iron content (RII), we have been able to show that there may be more abnormal iron deposition in the SN in IPD patients compared to HC based on RII mean susceptibility and volumes. It may also serve to be a more robust method for measuring iron content in disease states than methods which use the whole structure due to the general improvement of the correlation coefficients after thresholding.

Acknowledgements

The authors would like to acknowledge Sara Gharabaghi and Magnetic Resonance Innovations, India for assistance with data processing and preparation.

Funding

The author(s) received no specific funding for this work.

References

[1] Popescu BF, George MJ, Bergmann U, et al. Mapping metals in Parkinson's and normal brain using rapid-scanning X-ray fluorescence. Phys Med Biol 2009;54(3):651–63.
[2] Shulman JM, De Jager PL. Evidence for a common pathway linking neurodegenerative diseases. Nat Genet 2009;41(12):1261–2.
[3] Braak H, Del Tredici K, Rub U, de Vos RA, Jansen Steur EN, Braak E. Staging of brain pathology related to sporadic Parkinson's disease. Neurobiol Aging 2003;24(2):197–211.
[4] Damier P, Hirsch EC, Agid Y, Graybiel AM. The substantia nigra of the human brain. II. Patterns of loss of dopamine-containing neurons in Parkinson's disease. Brain 1999;122(Pt 8):1437–48.
[5] Koller WC, Montgomery EB. Issues in the early diagnosis of Parkinson's disease. Neurology 1997;49(1 Suppl 1):S10–25.
[6] Scherfler C, Esterhammer R, Nocker M, et al. Correlation of dopaminergic terminal dysfunction and microstructural abnormalities of the basal ganglia and the olfactory tract in Parkinson's disease. Brain 2013;136(Pt 10):3028–37.
[7] Balash Y, Korczyn AD. Vascular parkinsonism. Handb Clin Neurol 2007;84:417–25.
[8] Zarow C, Lyness SA, Mortimer JA, Chui HC. Neuronal loss is greater in the locus coeruleus than nucleus basalis and substantia nigra in Alzheimer and Parkinson diseases. Arch Neurol 2003;60(3):337–41.
[9] Braak H, Ghebremedhin E, Rub U, Bratzke H, Del Tredici K. Stages in the development of Parkinson's disease-related pathology. Cell Tissue Res 2004;318(1):121–34.
[10] Goetz CG, Fahn S, Martinez-Martin P, et al. Movement Disorder Society-sponsored revision of the Unified Parkinson's Disease Rating Scale (MDS-UPDRS): process, format, and clinimetric testing plan. Mov Disord 2007;22(1):41–7.
[11] Goetz CG, Tilley BC, Shaftman SR, et al. Movement Disorder Society-sponsored revision of the Unified Parkinson's Disease Rating Scale (MDS-UPDRS): scale presentation and clinimetric testing results. Mov Disord 2008;23(15):2129–70.
[12] Agid Y, Cervera P, Hirsch E, et al. Biochemistry of Parkinson's disease 28 years later: a critical review. Mov Disord 1989;4(Suppl. 1):S126–44.
[13] Javoy-Agid F, Ruberg M, Taquet H, et al. Biochemical neuropathology of Parkinson's disease. Adv Neurol 1984;40:189–98.
[14] Hallgren B, Sourander P. The effect of age on the non-haemin iron in the human brain. J Neurochem 1958;3(1):41–51.
[15] Wang Y, Butros SR, Shuai X, et al. Different iron-deposition patterns of multiple system atrophy with predominant parkinsonism and idiopathetic Parkinson diseases demonstrated by phase-corrected susceptibility-weighted imaging. AJNR Am J Neuroradiol 2012;33(2):266–73.
[16] Dashtipour K, Liu M, Kani C, et al. Iron accumulation is not homogenous among patients with Parkinson's disease. Parkinsons Dis 2015;2015:324843.
[17] Dexter DT, Carayon A, Javoy-Agid F, et al. Alterations in the levels of iron, ferritin and other trace metals in Parkinson's disease and other neurodegenerative diseases affecting the basal ganglia. Brain 1991;114(Pt 4):1953–75.
[18] Martin WR, Wieler M, Gee M. Midbrain iron content in early Parkinson disease: a potential biomarker of disease status. Neurology 2008;70(16 Pt 2):1411–7.
[19] Berg D, Roggendorf W, Schroder U, et al. Echogenicity of the substantia nigra: association with increased iron content and marker for susceptibility to nigrostriatal injury. Arch Neurol 2002;59(6):999–1005.
[20] Haacke EM, Miao Y, Liu M, et al. Correlation of putative iron content as represented by changes in R2* and phase with age in deep gray matter of healthy adults. J Magn Reson Imaging 2010;32(3):561–76.
[21] Haacke EM, Garbern J, Miao Y, Habib C, Liu M. Iron stores and cerebral veins in MS studied by susceptibility weighted imaging. Int Angiol 2010;29(2):149–57.
[22] Daugherty AM, Raz N. Appraising the role of iron in brain aging and cognition: promises and limitations of MRI methods. Neuropsychol Rev 2015;25(3):272–87.
[23] Rudko DA, Klassen LM, de Chickera SN, Gati JS, Dekaban GA, Menon RS. Origins of R2* orientation dependence in gray and white matter. Proc Natl Acad Sci U S A 2014;111(1):E159–67.
[24] Haacke EM, Ayaz M, Khan A, et al. Establishing a baseline phase behavior in magnetic resonance imaging to determine normal vs. abnormal iron content in the brain. J Magn Reson Imaging 2007;26(2):256–64.
[25] Bourekas EC, Christoforidis GA, Abduljalil AM, et al. High resolution MRI of the deep gray nuclei at 8 Tesla. J Comput Assist Tomogr 1999;23(6):867–74.
[26] Christoforidis GA, Bourekas EC, Baujan M, et al. High resolution MRI of the deep brain vascular anatomy at 8 Tesla: susceptibility-based enhancement of the venous structures. J Comput Assist Tomogr 1999;23(6):857–66.
[27] Ogg RJ, Langston JW, Haacke EM, Steen RG, Taylor JS. The correlation between phase shifts in gradient-echo MR images and regional brain iron concentration. Magn Reson Imaging 1999;17(8):1141–8.
[28] Yao B, Li TQ, Gelderen P, Shmueli K, de Zwart JA, Duyn JH. Susceptibility contrast in high field MRI of human brain as a function of tissue iron content. Neuroimage 2009;44(4):1259–66.
[29] Haacke EM, Liu S, Buch S, Zheng W, Wu D, Ye Y. Quantitative susceptibility mapping: current status and future directions. Magn Reson Imaging 2015;33(1):1–25.
[30] Du G, Liu T, Lewis MM, et al. Quantitative susceptibility mapping of the midbrain in Parkinson's disease. Mov Disord Off J Mov Disord Soc 2016;31(3):317–24.
[31] Guan X, Xuan M, Gu Q, et al. Regionally progressive accumulation of iron in Parkinson's disease as measured by quantitative susceptibility mapping. NMR Biomed 2015:30(4).
[32] Langkammer C, Pirpamer L, Seiler S, et al. Quantitative susceptibility mapping in Parkinson's disease. PLoS One 2016;11(9):e0162460.
[33] Murakami Y, Kakeda S, Watanabe K, et al. Usefulness of quantitative susceptibility mapping for the diagnosis of Parkinson disease. AJNR Am J Neuroradiol 2015;36(6):1102–8.
[34] Liu M, Liu S, Ghassaban K, et al. Assessing global and regional iron content in deep gray matter as a function of age using susceptibility mapping. J Magn Reson Imaging 2016;44(1):59–71.
[35] Liu S, Buch S, Chen Y, et al. Susceptibility-weighted imaging: current status and future directions. NMR Biomed 2017:30(4).
[36] Smith SM. Fast robust automated brain extraction. Hum Brain Mapp 2002;17(3):143–55.
[37] Abdul-Rahman HS, Gdeisat MA, Burton DR, Lalor MJ, Lilley F, Moore CJ. Fast and robust three-dimensional best path phase unwrapping algorithm. Appl Optics 2007;46(26):6623–35.
[38] Schweser F, Deistung A, Lehr BW, Reichenbach JR. Quantitative imaging of intrinsic magnetic tissue properties using MRI signal phase: an approach to in vivo brain iron metabolism? Neuroimage 2011;54(4):2789–807.
[39] Tang J, Liu S, Neelavalli J, Cheng YC, Buch S, Haacke EM. Improving susceptibility mapping using a threshold-based K-space/image domain iterative reconstruction approach. Magn Reson Med 2013;69(5):1396–407.
[40] Shrout PE, Fleiss JL. Intraclass correlations: uses in assessing rater reliability. Psychol Bull 1979;86(2):420–8.
[41] Wang JY, Zhuang QQ, Zhu LB, et al. Meta-analysis of brain iron levels of Parkinson's disease patients determined by postmortem and MRI measurements. Sci Rep 2016;6:36669.
[42] Dias V, Junn E, Mouradian MM. The role of oxidative stress in Parkinson's disease. J Parkinsons Dis 2013;3(4):461–91.
[43] Lotfipour AK, Wharton S, Schwarz ST, et al. High resolution magnetic susceptibility mapping of the substantia nigra in Parkinson's disease. J Magn Reson Imaging 2012;35(1):48–55.
[44] Barbosa JH, Santos AC, Tumas V, et al. Quantifying brain iron deposition in patients with Parkinson's disease using quantitative susceptibility mapping, R2 and R2.

Magn Reson Imaging 2015;33(5):559–65.
[45] Acosta-Cabronero J, Cardenas-Blanco A, Betts MJ, et al. The whole-brain pattern of magnetic susceptibility perturbations in Parkinson's disease. Brain 2017;140(1):118–31.
[46] Guan X, Xuan M, Gu Q, et al. Regionally progressive accumulation of iron in Parkinson's disease as measured by quantitative susceptibility mapping. NMR Biomed 2017;30(4).
[47] Guan X, Xuan M, Gu Q, et al. Influence of regional iron on the motor impairments of Parkinson's disease: a quantitative susceptibility mapping study. J Magn Reson Imaging 2017;45(5):1335–42.
[48] Li W, Wu B, Batrachenko A, et al. Differential developmental trajectories of magnetic susceptibility in human brain gray and white matter over the lifespan. Hum Brain Mapp 2014;35(6):2698–713.
[49] Ghassaban K, Liu S, Jiang C, Haacke EM. Quantifying iron content in magnetic resonance imaging. Neuroimage 2018. (S1053-8119(18)30357-4).